A Highly Sensitive Bolometer Structure With an Electrostatic-Actuated Signal Bridge

Tae-Sik Kim and Hee Chul Lee

***Abstract*—A novel bolometer structure has been proposed to achieve high detectivity. The detectivity is inversely proportional to the thermal conductance of a bolometer, and most of the thermal conductance is due to a metal wire, the placement of which is necessary for the reading of a signal. However, the thermal conductance of the proposed bolometer was unaffected by the thermal conductance of a metal wire. This is because a movable signal bridge was employed to lower the thermal conductance, thereby yielding a thermal conductance of 4.13 $\times$ 10^{-8} W/K. A measured detectivity of up to 4.23 $\times$ 10^{9} cm $\cdot$ Hz$^{1/2}$/W was attained at room temperature.**

***Index Terms*—Actuators, bolometers, infrared detectors, microelectromechanical devices, stress.**

I. Introduction

METAL films have promise for use as sensing materials for resistive bolometers, which have many anticipated uses in civilian and military applications. Although metal films have a low temperature coefficient of resistance (TCR, α) with respect to other kinds of materials, they display low $1/f$ noise characteristics [1], [2], thus making them suitable for use as sensing materials in resistive bolometers. To achieve a high detectivity, it is desirable to lower the thermal conductance of a bolometer. However, the thermal conductance G_{leg} of a traditional metal bolometer structure is usually larger than 1×10^{-7} W/K (in a two-level structure) due to the use of metal wires located on the supporting legs, which are used for reading a signal [3]. A novel bolometer structure is proposed in this study, wherein the thermal conductance is unaffected by the thermal conductance of the metal wire. This is facilitated by separating the metal wire and the supporting leg into a bridge, and a post incorporating the leg, respectively.

II. Principle

Fig. 1 shows a schematic drawing of the proposed bolometer structure. The bolometer includes a resistor, a readout circuit on the substrate, a quarter-wave resonant cavity between the resistor and the reflector, two posts to mechanically support the resistor, and two bridges to electrically connect the resistor to the readout circuit. The resistance of the resistor is changed by temperature, and the quarter-wave resonant cavity increases the absorption of infrared radiation (IR).

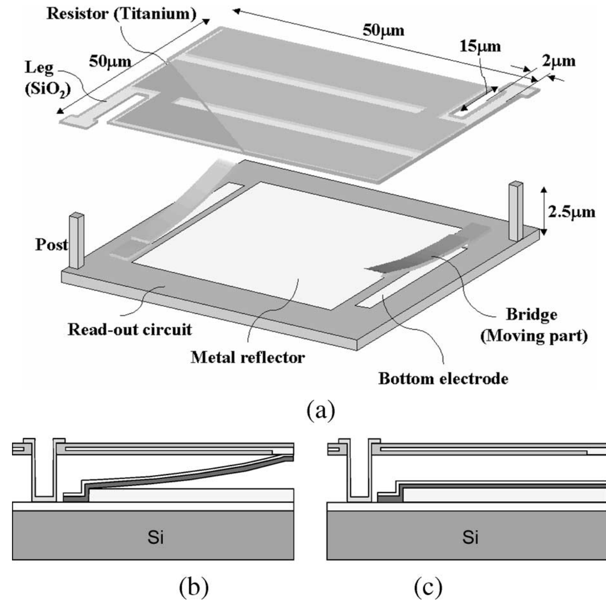

Fig. 1. Schematic diagram of the proposed bolometer. (a) Cutaway view of the device. (b) Cross-sectional view of the bent signal bridge connected with the resistor by residual stress. (c) Cross-sectional view of the bridge disconnected with the resistor by applying electric field.

Fig. 2 shows the temperature change (ΔT: the temperature difference between the resistor and the substrate) of the resistor during a given time frame of 33 ms, which is from a frame rate of 30 Hz. A time frame comprises three modes of operation, namely: 1) IR absorption during the t_a period; 2) a reading of the resistance change by the IR during the t_b period; and 3) a discharging of the temperature change into the substrate during the t_c period after reading. The bridges are composed of a metal and an insulator. Controlled residual stresses of the two layers warp a bridge upward, which normally provides contact between the two bridges and the resistor. The two bridges are electrically open from the resistor while absorbing IR. This is done by the application of an electric field between the metal wire of the bridge and the bottom electrode on the substrate. Therefore, the thermal conductance G_{leg} through the two posts including the two legs is much lower than that of a conventional bolometer structure while absorbing IR. The two bridges then continue to make contact with the resistor while reading the resistance change and completely removing the temperature change by way of the two bridges after reading. These steps are performed repeatedly.

Manuscript received November 22, 2005; revised June 12, 2006. The review of this paper was arranged by Editor K. Najafi.

The authors are with the Department of Electrical Engineering and Computer Science, Korea Advanced Institute of Science and Technology, Daejeon 305-701, Korea (e-mail: kimtaesik@kaist.ac.kr).

Digital Object Identifier 10.1109/TED.2006.880826

0018-9383/$20.00 © 2006 IEEE

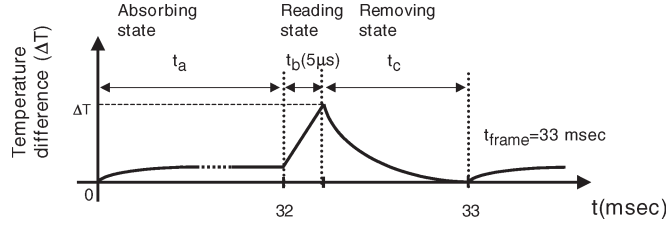

Fig. 2. Temperature change (ΔT: the temperature difference between the resistor and the substrate) of the resistor during a time frame.

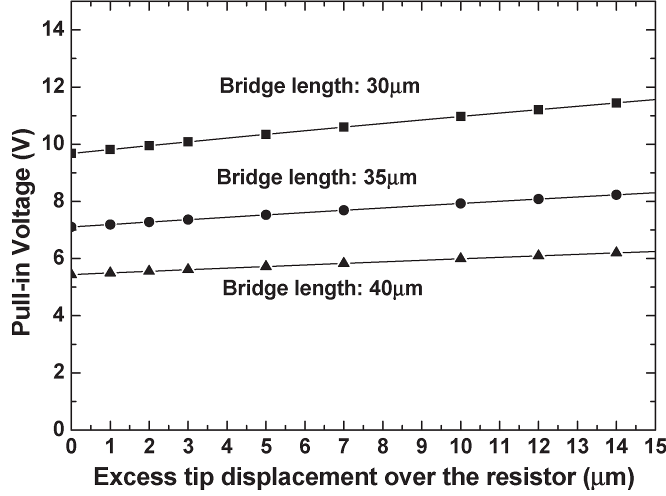

Fig. 3. Calculated results of the pull-in voltage versus excess tip displacement over the resistor. The resistor is spaced at a height of 2.5 μm.

III. Design

This bolometer employs a titanium metal film with a TCR of approximately 0.26%/K. The titanium film is encapsulated between two layers of silicon dioxide in a pixel size of 50 μm. Because of its low resistivity, a serpentine structure is used to achieve a resistance of 40 kΩ.

A movable signal bridge, actuated by electrostatic force, is a key component in the proposed bolometer. It is important for the signal bridge driven in a low pull-in voltage to be designed. Thus, because a low pull-in voltage is achieved at a low value of the Young's modulus from the viewpoint of material property [4], aluminum as a metal structure and silicon dioxide as an insulator are selected for use. For the proposed structure (as shown in Fig. 1), although the tip of the bridge is designed to warp over 2.5 μm, it stops when it reaches 2.5 μm. This is the distance between the resistor and the substrate. In this way, the bridge has a tensile force corresponding to excess tip displacement over 2.5 μm. Under various types of excess tip displacements, the pull-in voltage is calculated for different bridge lengths (see Fig. 3) using the design parameters (i.e., 5-μm-wide bridge, 600-Å-thick aluminum, 2000-Å-thick silicon dioxide, 500-Å-thick silicon nitride used as an insulator on the bottom electrode, and 1000-Å-thick polyimide between the bridge and the silicon nitride [5], [6]) and the following equation:

$$V_{\rm pi}^2 = \frac{1}{\varepsilon_0 h} \frac{\left(\mathrm{EI} \int_0^L \left[\frac{d^2 g(x)}{dx^2}\right]^2 dx + N \int_0^L \left[\frac{dg(x)}{dx}\right]^2 dx\right)}{\int_0^L \frac{g^2(x)}{\left(\frac{d_1}{\varepsilon_{r1}} + \frac{d_2}{\varepsilon_{r2}} + d_{\rm air} + \delta(x) - c_{\rm pi} g(x)\right)^3} dx} \quad (1)$$

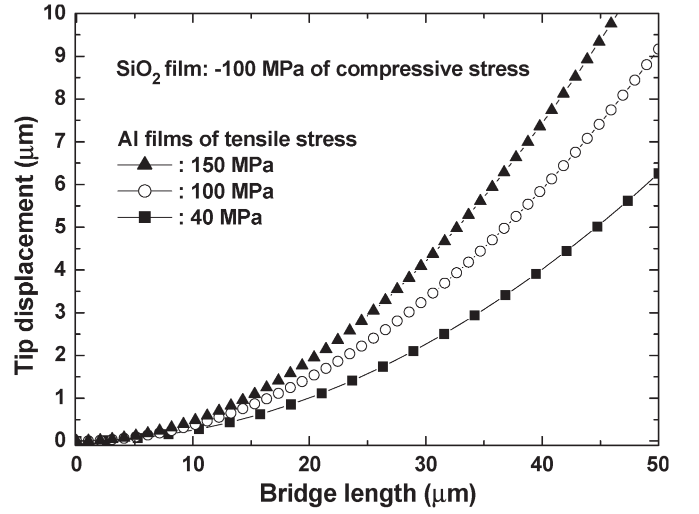

Fig. 4. Tip displacement of the bridge versus the bridge length with SiO_2 intrinsic stress of -100 MPa of compressive for various kinds of Al films of tensile stress.

where $V_{\rm pi}$ denotes the pull-in voltage of the cantilever; h is the width; EI is the bending stiffness; L is the bridge length; N is the tensile force; $d1$ and $d2$ are the thickness of the insulator of the signal bridge and the insulator on the bottom electrode, respectively; $d_{\rm air}$ is the distance between the two insulators; ε_0 is the dielectric constant in air; ε_{r1} and ε_{r1} are the dielectric constant of the insulator of the bridge and the insulator on the bottom electrode, respectively; $\delta(x)$ is the shape of the signal bridge as a function of the position x; and $c_{\rm pi}g(x)$ is the deflection profile of a uniformly loaded beam. It was determined that a change of pull-in voltage depending on the excess tip displacement of the bridge is minor, but a change of pull-in voltage depending on the length of the bridge is large, which reveals that the bridge length rather than the excess tip displacement more efficiently influences pull-in voltage. Hence, to obtain a pull-in voltage of less than 10 V, the length here is designed to be in the range of 35–40 μm.

Analytical calculations to find the tip displacement depending on the residual stress of each layer were performed using (2), (3), and the aforementioned design parameters, and the results of the tip displacement versus the bridge lengths are shown in Fig. 4. The findings show that the tip displacement of the bridge can be adjusted by controlling the residual stresses of each layer [7], [8], i.e.,

$$\rho = \frac{hE_2 \left(3m + K\left[n(1+n)^2\right]^{-1}\right)}{6(m\sigma_2 - \sigma_1)} \quad (2)$$

$$\zeta = \rho\left(1 - \cos(L/\rho)\right) \quad (3)$$

where

$$K = 1 + 4mn + 6mn^2 + 4mn^3 + m^2n^4$$

$$m = E_1/E_2 \text{ and } n = h_1/h_2$$

ζ is the deflection perpendicular to the unreleased position, L is the bridge length, and ρ is the radius of curvature. The values of E_1 and E_2 are 75 and 65 GPa, respectively.

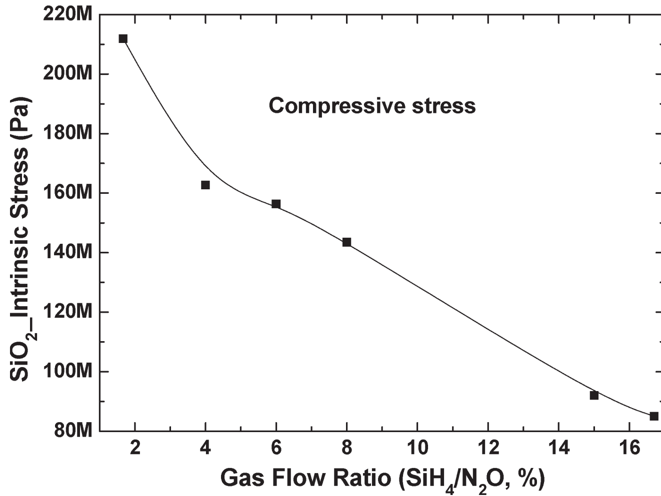

Fig. 5. Measured results of the intrinsic stress of the silicon dioxide film as a function of gas flow ratio (SiH_4/N_2O) at process conditions: power (20 W), process pressure (650 mtorr), and deposition temperature (150 °C).

A device containing a membrane made of films is often damaged due to the large stress of the membrane [9]. Thus, to reduce the stress, a stress compensation method is utilized [10]. In keeping with this method, a sandwich structure of $SiO_2/Ti/SiO_2$ is used for the absorber, which also encompasses the resistor. From the measured results of the intrinsic stress of the SiO_2 film versus gas flow ratio at a deposition temperature of 150 °C (as shown in Fig. 5), it is found that the intrinsic stress of the SiO_2 film is about −85 MPa of compressive stress at a gas flow ratio of 17%. However, the residual stress of the upper SiO_2 film is the sum of the intrinsic stress of the SiO_2 and the thermal stress (of −86 MPa) of compressive stress due to a mismatch between the thermal expansion coefficient of the Ti film and the SiO_2 film, and this thereby yields the residual stress of −171 MPa of compressive stress. To make the membrane flat by reducing its residual stress for a thickness of the membrane at 600-Å SiO_2/100-Å Ti/200-Å SiO_2, the required stress of the Ti film is approximately 852 MPa (tensile stress) [11], [12].

The detectivity is inversely proportional to the thermal conductance G_{leg}. Thus, to obtain a thermal conductance G_{leg} as low as possible through the two posts incorporating the two legs, a leg made of silicon dioxide was designed with a thickness of 800 Å, a width of 2 μm, and a length of 15 μm, yielding the thermal conductance down to 2.94 × 10^{-8} W/K using the material properties (Table I) and the following equation:

$$G = k\frac{wd}{l} \quad \text{(in watts per kelvin)} \tag{4}$$

where k is the thermal conductivity, w is the width, d is the thickness, and l is the length. The thermal mass C of the absorber must be made low enough to meet a response time requirement of about 10 ms. From the above designed values [lower SiO_2 (600 Å)/upper SiO_2 (200 Å)] and the assumption of a 100-Å-thick titanium film, the thermal mass of the membrane was calculated to be 3.6 × 10^{-10} J/K using the equation

$$C = \rho c V \quad \text{(in joules per kelvin)} \tag{5}$$

TABLE I
MATERIAL PROPERTIES

	ρ(Kg/m³)	c(J/Kg K)	G (W/mK)
SiO_2	2220	745	1.38
Ti	4500	522	21.9

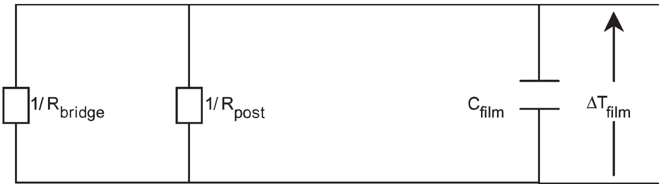

Fig. 6. Simple electrical discrete-element model of the bolometer.

where ρ is the density, c is the specific heat, and V is the volume, and using the material properties (Table I). Thus, the thermal time response τ is approximately 12 ms by the following equation:

$$\tau = \frac{C}{G}. \tag{6}$$

The thermal conductance G_{bridge} of the bridge needs to be designed while considering two factors. First, when the bridges make contact with the resistor to read the resistance change during the period t_b (5 μs), the increase in temperature brought on by the absorbed IR leaks from the resistor through the two bridges, inducing a decrease of resistance change. In this case, the proposed bolometer structure can be represented by a simple electrical discrete-element model as shown in Fig. 6, where $1/R_{\text{bridge}}$, $1/R_{\text{post}}$, and C_{film} are the thermal conductance of the two bridges and the post and thermal capacitances of the absorber, respectively. In addition, $1/R_{\text{bridge}}$ is a variable parameter, and C_{film} is 3.6 × 10^{-10} J/W. From the simple model and the assumption of $1/R_{\text{post}} \ll 1/R_{\text{bridge}}$, the time constant follows from the thermal conduction and thermal capacitance, i.e.,

$$\tau = R_{\text{bridge}} C_{\text{film}}. \tag{7}$$

The charged temperature dissipated through the $1/R_{\text{bridge}}$ can be expressed by

$$\Delta T_{\text{film}}(t) = \Delta T_0 \exp(-t/\tau) \tag{8}$$

where ΔT_0 is the charged temperature at $t = 0$. Using (8), temperature leakage was calculated as shown in Fig. 7. Fig. 7(a) shows this temperature leakage as a function of the reading time for various thermal conductances. It is found in Fig. 7(a) that a thermal conductance of 4.1 × 10^{-6} W/K of the two bridges causes the temperature of the resistor to leak through the bridges by 5% during the period. To obtain a high detectivity, this temperature leakage should be minimized. Therefore, the thermal conductance of the two bridges is designed to be less than 4.1 × 10^{-6} W/K. The second factor has to do with the fact that the temperature change increases due to the self-heating effect of the bias current while reading the resistance change [13]. A maximum allowable temperature change of 30 °C is

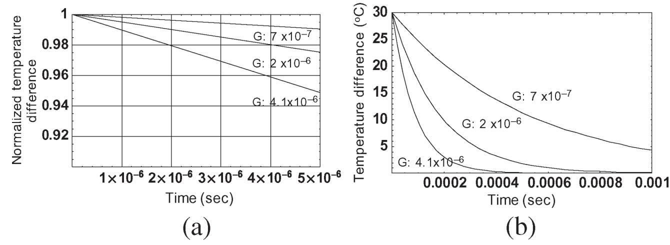

Fig. 7. Change of the temperature difference. (a) During the reading time. (b) During the removing time for various thermal conductances of the signal bridge.

TABLE II
THICKNESS OF SILICON DIOXIDE AND ALUMINUM CORRESPONDING TO THERMAL CONDUCTANCE FOR 35 μm IN BRIDGE LENGTH AND 5 μm IN BRIDGE WIDTH

Al thickness (Å)	SiO_2 thickness (Å)	Response time (μsec)	G (W/K)
600	2000	87.6	4.1x10-6
300	1500	~180	2.07x10-6
100	1000	514.2	7.1x10-7

selected to prevent unintentional changes in the TCR and the resistance of the resistor [14]. Thus, to prevent an accumulative increase in temperature change for a sequence of time frames, the temperature change should be eliminated during the period t_c (1 ms) after reading. Using (8), the temperature change during the period can be calculated as shown in Fig. 7(b). Fig. 7(b) shows that a bridge with a thermal conductance of 2.1×10^{-6} W/K makes the temperature change almost zero at the end of the period. This finding reveals that the two bridges had to be designed to have a thermal conductance larger than the thermal conductance of 2.1×10^{-6} W/K, which is enough to eliminate the temperature change during a period. Finally, according to the above statement, to satisfy the two factors, the thermal conductance is designed to fit between 4.1×10^{-6} and 2.1×10^{-6} W/K, and the aluminum thickness and the silicon dioxide thickness are designed in ranges of 300–600 Å and 1500–2000 Å, respectively, as shown in Table II.

Simulation results using the Essential–Macleod [15] program for the absorptance of the resonant cavity reveal that an average absorptance of 70% at wavelengths ranging from 8 to 12 μm is achieved at a Ti thickness of 100 Å as shown in Fig. 8. The fill factor of the proposed structure is approximately 75%.

There are mainly three noise components in the bolometer: 1) the Johnson noise, 2) the temperature fluctuation, and 3) the background fluctuation noise. The Johnson noise component of the total noise is given by

$$V_J = \sqrt{4k_B TR\Delta f} \tag{9}$$

where k_B is the Boltzmann's constant, T is the bolometer temperature, R is the bolometer resistance, and Δf is the bandwidth corresponding to the integration time. The temperature fluctuation noise component is expressed by

$$\overline{V_{\rm tf}^2} = \frac{4k_B TG\Re_V^2}{\varepsilon} \tag{10}$$

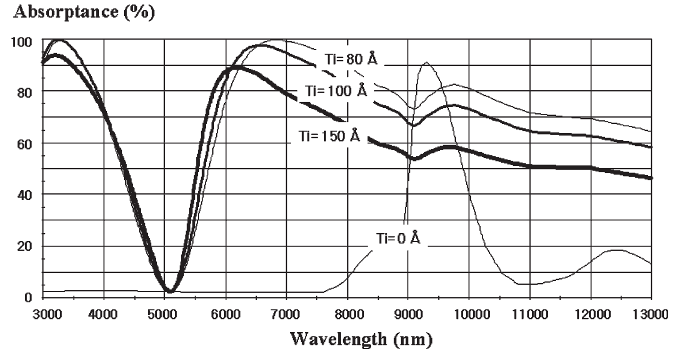

Fig. 8. Simulation results of absorptance to the membrane with lower SiO_2 (600 Å)/upper SiO_2 (200 Å) for various thicknesses of a titanium film.

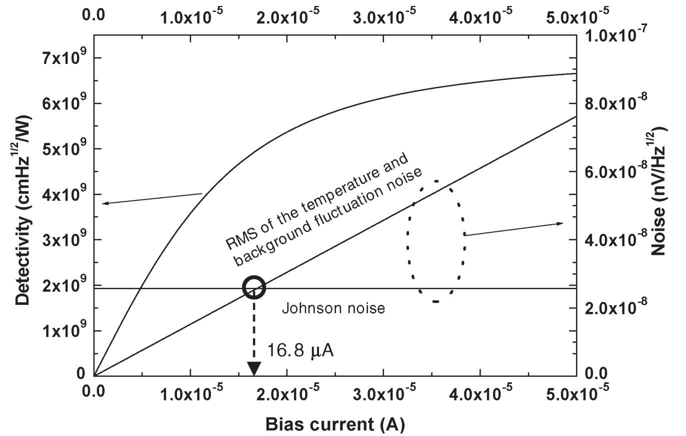

Fig. 9. Characteristics of detectivity and noises as a function of bias current.

where $\Re_V$ is the responsivity, and ε is the emissivity. The mean square background noise voltage is given by

$$\overline{V_{\rm bf}^2} = 8A\varepsilon\sigma k_B \left(T^5 + T_B^5\right) \Re_V^2. \tag{11}$$

Here, A is the area of the detector, σ is the Stefan–Boltzmann's constant, and T and T_B are the bolometer temperature and the background temperature, respectively. The total mean square noise voltage (i.e., V_n^2) is obtained by adding together the four contributions, i.e.,

$$\overline{V_n^2} = \overline{V_J^2} + \overline{V_{\rm tf}^2} + \overline{V_{\rm bf}^2}. \tag{12}$$

Because the Johnson noise of the three noise components is dominant at low current level, the detectivity D^* linearly increases with the bias current at low current level and starts to become saturated around a current of 16.8 μA, at which the root-mean-square (rms) value of the temperature fluctuation and the background fluctuation noise voltage is calculated to be equal to the Johnson noise voltage by using (9)–(14) and the above designed parameters as shown in Fig. 9. This occurs because the temperature fluctuation and the background fluctuation noise voltage are directly proportional to the bias current, but the Johnson noise is independent of the bias current as shown in (9)–(11), and (13). Therefore, a bias current larger than 16.8 μA is selected, but this increased bias current raises the temperature of the resistor for the reading state through a self-heating effect. Thus, the bias current must be limited, so that it does not exceed the maximum allowable temperature

TABLE III
DESIGN PARAMETERS FOR THE PROPOSED BOLOMETER STRUCTURE

R (kΩ)	Current (mA)	TCR (%/K)	Absorptance (%)	Thermal conductance of the leg (W/K)	Thermal conductance of the signal bridge (W/K)	Response time (msec)	Fill-factor (%)
40	0.23	0.26	70	2.94 x 10^{-8}	4 x 10^{-6}	12	75

change of 30 °C. Therefore, the bias current was designed to be 0.23 mA, at which the temperature change is 30 °C. The Johnson, temperature fluctuation, and background fluctuation noise voltages are estimated to be 25.7, 310.7, and 162.3 $\mathrm{nV/Hz^{1/2}}$ [16], respectively, for the detector and background temperature of 300 K.

From the assumption that the IR power varies at a slow rate compared with $1/2\pi\tau$, the equations of the responsivity and the detectivity can be expressed, respectively, as

$$\Re_V = \frac{i\alpha R\varepsilon}{G_{\mathrm{leg}}} \tag{13}$$

$$D^* = \frac{\Re_V\sqrt{\Delta f A}}{V_n} \tag{14}$$

where ε is the emissivity, V_n is the total noise voltage, i is the bias current, and Δf is the noise bandwidth. Using the designed values in Table III, the calculated detectivity of the proposed bolometer reached up to 7×10^9 $\mathrm{cm \cdot Hz^{1/2}/W}$ due to the lower thermal conductance G_{leg}, high absorptance, and high fill factor at room temperature.

IV. FABRICATION AND MEASUREMENT RESULTS

Fig. 10 shows the fabrication procedure of the proposed bolometer. A silicon dioxide layer was deposited to cover the substrate and, thus, electrically isolate the bottom electrode from the substrate. Then, a 200-Å-thick Cr adhesion layer and a 1500-Å-thick Au layer were deposited to form the bottom electrode, and the bottom electrode was passivated with a silicon nitride layer as shown in Fig. 10(a) and (b). A polyimide film used as a sacrificial layer was coated and cured at a temperature of 300 °C [Fig. 10(c)]. The bridge, which is a movable part to connect the readout circuit with the resistor, was made of 600-Å-thick SiO_2 deposited at a temperature of 300 °C and 2000-Å-thick Al [see Fig. 10(d)]. An Au metal was deposited on the edge of the Al film used as the signal bridge to protect a contact region from oxidation [see Fig. 10(e)]. Then, to form a quarter-wave resonant cavity, a 2.5-μm-thick polyimide was coated as a sacrificial layer and cured at a temperature of 200 °C [see Fig. 10(f)]. The first SiO_2 film composing the absorber was deposited by using plasma-enhanced chemical vapor deposition (PECVD) at a temperature of 150 °C, and a contact window was etched away. An Au metal was deposited on the contact window, where the signal bridge makes contact with, and then, the Ti metal used as the resistor was formed as shown in Fig. 10(g) and (h). Fig. 10(i) shows the second SiO_2 film deposited on the Ti film. An Al metal was deposited to form the post supporting the absorber [see Fig. 10(j)]. Then, the process defining a pixel followed. The final step is to release the membrane and the bridge by etching the polyimide [see Fig. 10(k)].

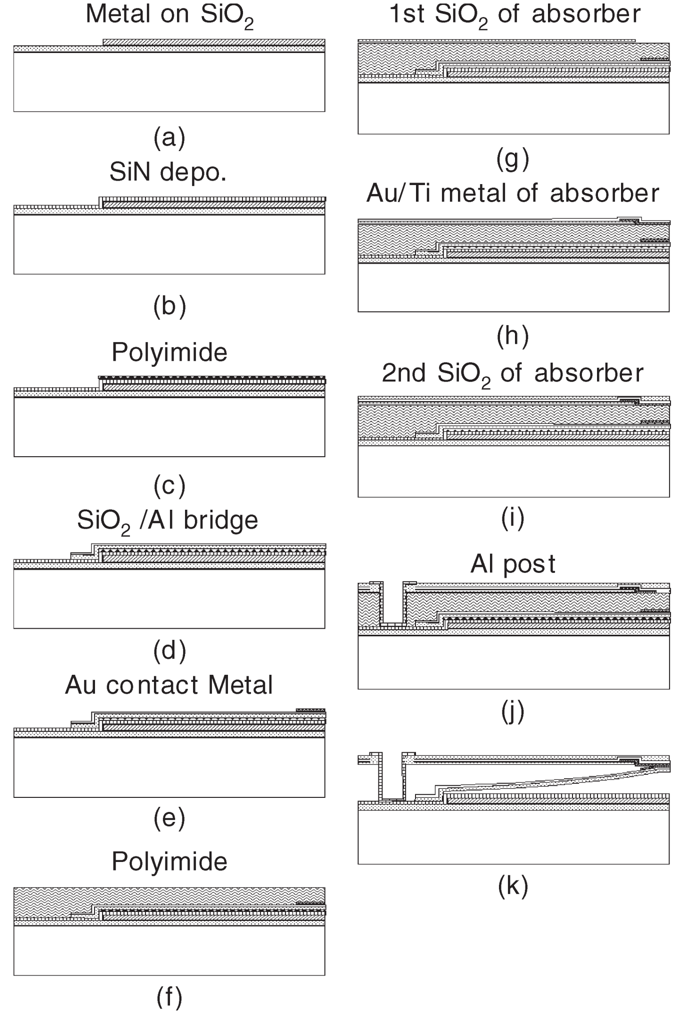

Fig. 10. Fabrication procedure of the proposed bolometer.

The signal bridge is composed of the aluminum and the silicon dioxide film, and therefore, stresses in the two films were investigated (as shown in Fig. 11). Using the aluminum film of 130 MPa of tensile stress and the silicon dioxide film of −124.6 MPa of compressive stress, the signal bridge was fabricated. Fig. 12 shows the calculated and measured results of the tip displacement of the bridge versus the bridge length, as well as the scanning electron microscopy (SEM) image of the fabricated bridge. Fig. 12(a) shows the increasing tendency of the measured results to agree with the calculated results at regular intervals. The discrepancy may be caused by the difference in the structural dimensions between the design and the fabrication. The SEM image shows a signal bridge in length

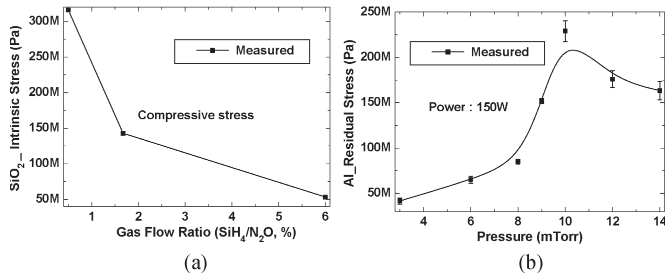

Fig. 11. Measured stress characteristics. (a) Intrinsic stress of the SiO_2 film at PECVD process conditions as follows: power (20 W), process pressure (650 mtorr), process temperature (300 °C). (b) Residual stress of the dc sputtered aluminum film as a function of process pressure.

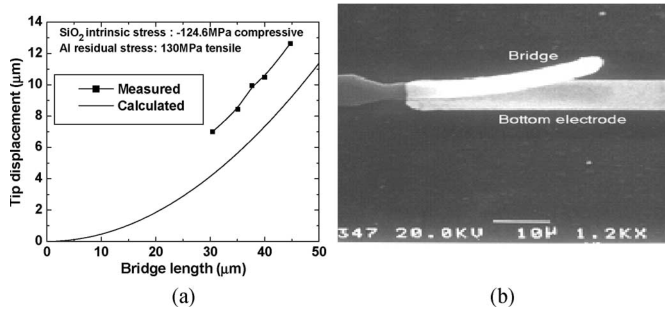

Fig. 12. (a) Calculated and measured results of tip displacement versus the bridge length. (b) SEM image of the fabricated signal bridge.

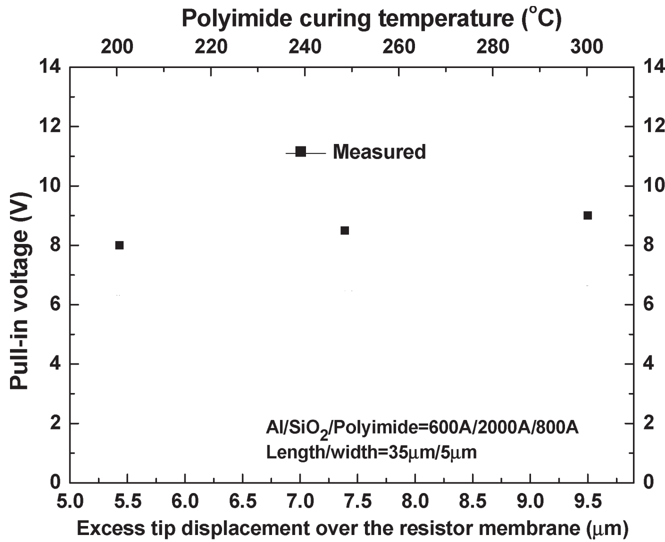

Fig. 13. Pull-in voltage versus excess tip displacement causing tensile force for the fabricated device with bridge length of 35 μm and Al/SiO_2 thickness of 600 Å/2000 Å.

of 35 μm and in tip displacement of 8 μm. It was found that a required tip displacement was to be achieved by adjusting the residual stresses of each layer.

The pull-in voltage of the fabricated signal bridge was measured. The curing temperature of the 2.5-μm-thick polyimide film serving as a sacrificial layer changes the stress of the Al film used as the metal structure of the signal bridge. This causes a transformation of the tip displacement of the signal bridge. As a result, the pull-in voltage is altered by this transformation of the tip displacement. Fig. 13 shows the measured pull-in voltages depending on three different curing temperatures

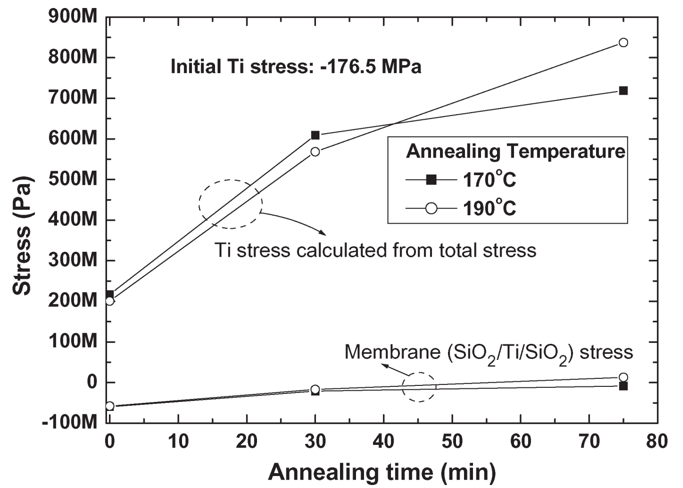

Fig. 14. Membrane $(SiO_2/Ti/SiO_2)$ and Ti stress as a function of annealing time at 170 °C and 190 °C, respectively.

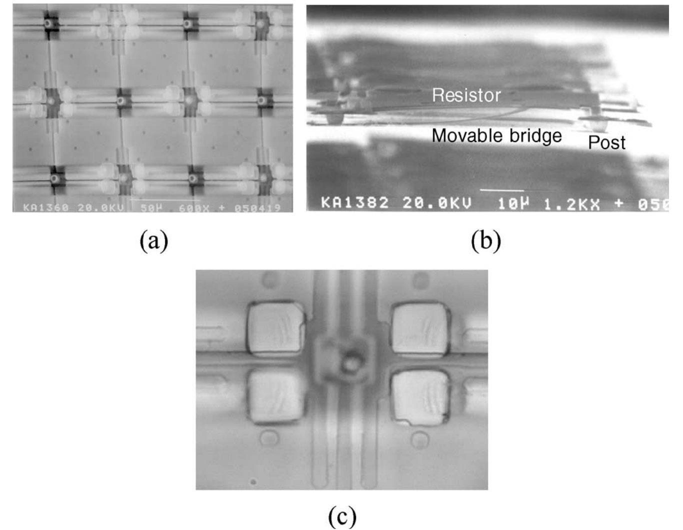

Fig. 15. SEM images and photomicrograph of the fabricated bolometer. (a) Top view of the fabricated bolometer array. (b) Enlarged picture of the bridge and post. (c) Photomicrograph of the contact region between the signal bridge and the resistor.

(i.e., 200 °C, 250 °C, and 300 °C). It was found that the change of the pull-in voltage was slight and that the pull-in voltages were less than 10 V in every case.

A suspended absorber composed of $SiO_2/Ti/SiO_2$ layers was released by O_2 plasma etching of a 2.5-μm-thick polymide film. The Ti film with −176.5 MPa of compressive stress was used for the membranes. The initial Ti stress of −176.5 MPa turned into a tensile stress of nearly 200 MPa due to the effect caused by depositing SiO_2 on the Ti layer at a temperature of 150 °C. However, the required stress of the Ti film was approximately 852 MPa of tensile stress to make the membrane flat. Therefore, the membranes were thermally annealed at 170 °C and 190 °C to increase the stress of Ti film in tensile. As a result, stress-free membranes were obtained, as shown in Fig. 14.

Fig. 15 shows the SEM images of the fabricated bolometer array. Its pixel size is $50 \times 50\ \mu m^2$. There are four etching holes to a unit cell to enhance the release process. Fig. 15(c) shows that a thin gold film was deposited at the contact region to

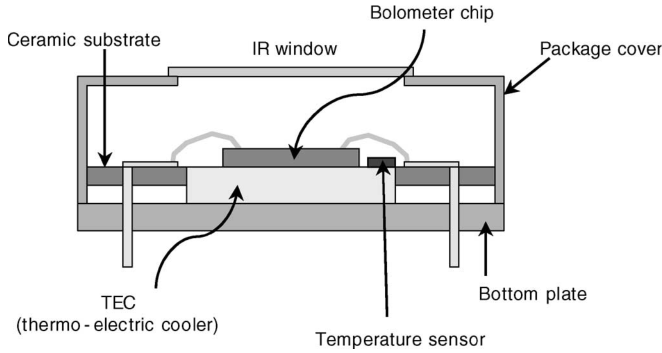

Fig. 16. Schematic diagram of a vacuum package.

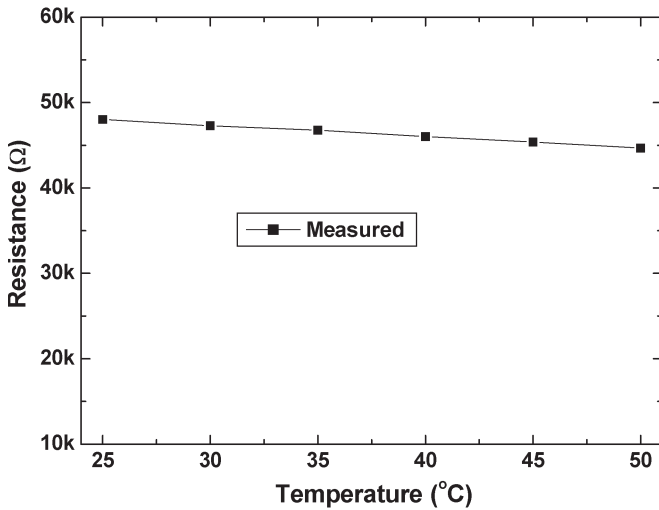

Fig. 17. Resistance changes as a function of temperature for the measurement of the TCR value.

reduce contact resistance between the signal bridge and the resistor. The bridge was bent upward and connected with the resistor at the end of the release process. Also, it is clearly shown that the resistor is suspended at a height of 2.5 μm by the two posts, and the released membrane is suspended with a high flatness.

Some thermal and optical properties for the fabricated bolometers were measured. Fig. 16 shows the schematic diagram of a vacuum package for the measurement. The bolometer was mounted on thermoelectric cooler (TEC) to maintain a constant temperature of the bolometer within better than about 0.05 K. The width and the length of the fabricated Ti resistor were about 15 and 116 μm, respectively, and its sheet resistance was changed from 1.3 to 6 $\mathrm{k}\Omega/\mathrm{sq}$ after thermal annealing at 170 °C for 70 min, which led to a resistance of around 46 kΩ. The measured resistances are shown in Fig. 17 as a function of temperature, and therefore, the TCR value was measured to be -0.275%/K at 25 °C from the following equation:

$$\alpha = \frac{dR}{R\,dT}. \tag{15}$$

The measured TCR of the Ti film deposited at a condition of approximately -176.5 MPa of compressive stress shows a negative value, which means that the properties of the Ti film used as the resistor are similar to those of the semiconductor.

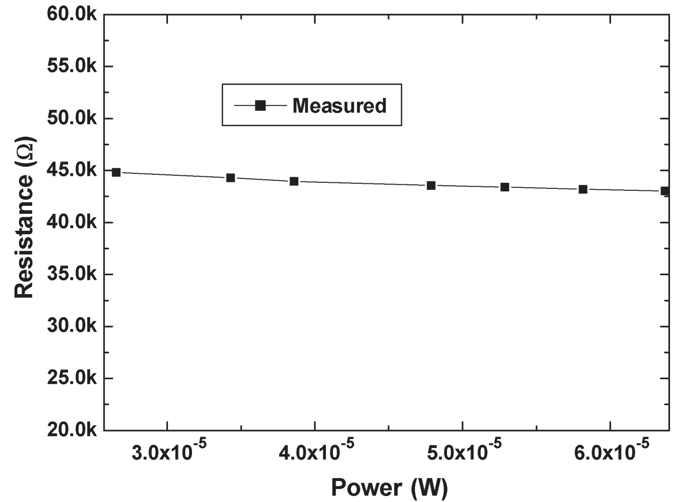

Fig. 18. Variation of the resistor versus biased power for the measurement of the thermal conductance G_{bridge}.

Therefore, it is expected that the $1/f$ noise of the bolometer will be higher than the $1/f$ noise of the other metal-type bolometers.

To determine the thermal mass of the absorber including the resistor, the thermal conductance G_{bridge} and the response time of the signal bridge were first measured by applying an electrical bias through the signal bridge. The heat balance equation due to applied electrical bias can be defined as

$$C\frac{d(\Delta T)}{dt} + G(\Delta T) = IV. \tag{16}$$

The solution of (16) is

$$\Delta T = \frac{IV}{G}\left(1 - e^{-t/\tau}\right) \tag{17}$$

where τ is the response time. Provided that $t \gg \tau$, (17) can be expressed as

$$\Delta T = \frac{IV}{G}. \tag{18}$$

Substituting $\Delta T = IV/G$ into (19) results in

$$R(T) = R(T_o)\left(1 + \alpha(T - T_o)\right) \tag{19}$$

$$R(T) = R(T_o)\left(1 + \frac{\alpha}{G}IV\right). \tag{20}$$

By fitting (20) to the measured R–IV curve, G_{bridge} can be extracted. Fig. 18 shows the measured resistance as a function of applied power. Using this method, the thermal conductance was estimated to be 3×10^{-6} W/K.

Also, the response time can be obtained by finding the change in the resistance of the resistor during a shorter time than the response time after applying the electrical bias through the signal bridge. Provided that $t \ll \tau$, (17) can be expressed as

$$\Delta T = \frac{IV}{G}\frac{t}{\tau}. \tag{21}$$

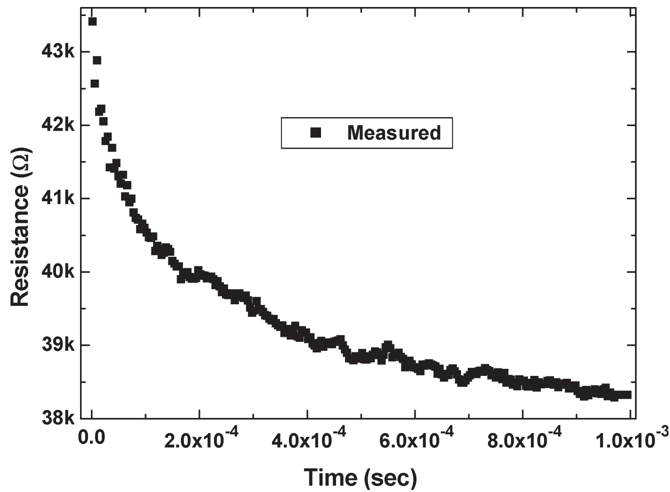

Fig. 19. Measured resistances as a function of time for the measurement of the thermal response time.

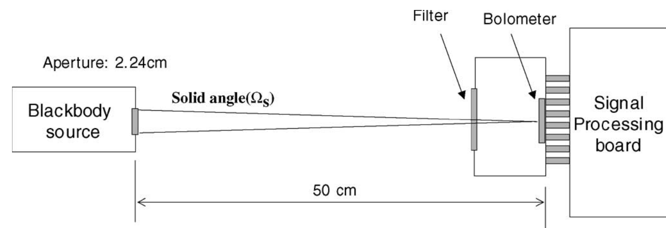

Fig. 20. Schematic diagram of measurement setup for responsivity.

Substituting $\Delta T = (IVt)/(G\tau)$ into (19) results in

$$R(T) = R(T_o)\left(1 + \alpha \frac{IV}{G}\frac{t}{\tau}\right). \quad (22)$$

The change of the resistance was measured (as shown in Fig. 19) as a function of time. By fitting (22) to the R–T curve, the response time was extracted and was determined to be 150 μs. The factors of the thermal conductance and the response time were used together for estimating the thermal mass of the absorber including the resistor by (6), and this yielded an estimated thermal mass of 4.5 $\times$ 10^{-10} J/K.

Fig. 20 shows the schematic diagram of the optical measurement setup for responsivity. The bolometer is mounted within a vacuum package with an ambient pressure lower than 20 mtorr, which has a germanium-coated window to pass specific wavelengths. The responsivity is defined as the ratio of the output signal to the input radiant power on the bolometer, i.e.,

$$\Re_V = \frac{\Delta \text{ Output signal}}{\Delta \text{ Input radiant power}} = \frac{\Delta V}{EA} \quad \text{(in volts per watt)} \quad (23)$$

where E is the incidence of incident power per unit collector area, and A is the pixel area. The change of the output voltage was measured to be 1.122 mV by varying the temperature of the blackbody from 300 to 900 K for a bias voltage of 1 V. Fig. 21 shows the transmittance characteristic of the filter, which has a transmittance of more than 50% at wavelengths ranging from 4 to 16 μm. For the temperature of the blackbody

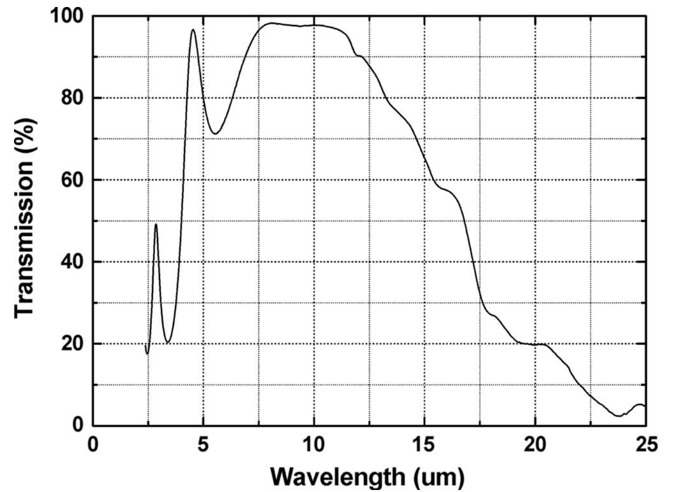

Fig. 21. Optical property of the germanium-coated window.

and the wavelength range of the filter, the incident power on the bolometer can be calculated by

$$E = \frac{\Omega_s}{\pi}\eta M \quad \text{[in watts per square centimeter]} \quad (24)$$

$$\Omega_s = \pi \frac{r^2}{R^2 + r^2} \quad (25)$$

$$M = \int_{\lambda_1}^{\lambda_2} \frac{2\pi hc^2}{\lambda^5 [e^{hc/\lambda kT} - 1]} d\lambda \quad \text{[in watts per square centimeter]} \quad (26)$$

where Ω_s is the solid angle for a round aperture, r is the radius of the aperture, R is the distance between the blackbody and the bolometer, η (0.8) is the transmittance, and M is the exitance. The incident power was calculated to be 2.4096 $\times$ 10^{-8} W. Using the change of the output voltage and the incident power, a responsivity of 4.6563 $\times$ 10^4 V/W was estimated.

By comparing the measured responsivity with the responsivity equation of (13), the thermal conductance $G_{\rm leg}$ through the two legs can be obtained, and it yielded a thermal conductance of 4.13 $\times$ 10^{-8} W/K. In addition, using (6), a response time of 10 ms of the leg was calculated using the thermal mass and the thermal conductance of the two legs.

Fig. 22 shows measurements of the thermal noise and $1/f$ noise current spectral density of the bolometer along with its calculated thermal noise current spectral density. From these results, the values of the $1/f$ noise parameter k and β in $1/f^\beta$ were 5.39 $\times$ 10^{-12} and 0.84, respectively. In the case of a noise bandwidth of 100 kHz, the thermal noise was 8.47 μV, and the $1/f$ noise voltage was 7.87 μV. In addition, the temperature fluctuation noise and the background fluctuation noise must both be considered because the thermal conductance of the two legs is lower. The temperature fluctuation noise and the background fluctuation noise were estimated to be 9.53 and 4.2 μV [16], respectively. The resulting total noise voltage was determined to be 15.57 μV.

The specific detectivity of the fabricated bolometer can be estimated using the measured responsivity and noise characteristics with the parameters as follows: an area of

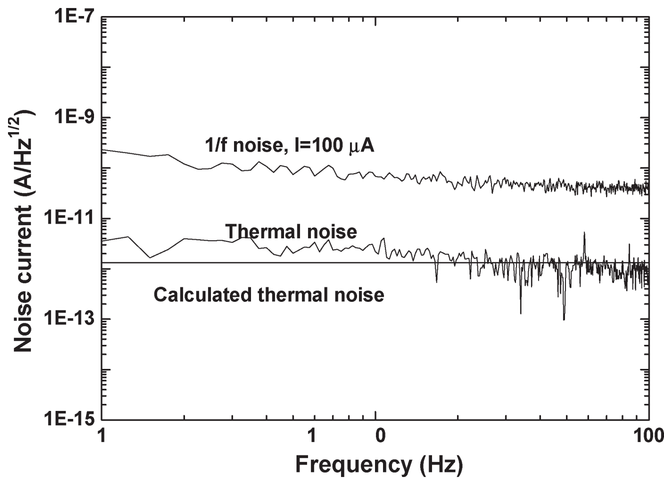

Fig. 22. Measured $1/f$ and thermal noise current spectral density, and calculated thermal noise spectral density.

$50 \times 50\ \mu m^2$, a fill factor of 80%, and a noise bandwidth of 100 kHz. The estimated detectivity of up to $4.23 \times 10^9\ \mathrm{cm} \cdot \mathrm{Hz}^{1/2}/\mathrm{W}$ was attained at room temperature, which compares favorably to those of bolometers of $5 \times 10^8\ \mathrm{cm} \cdot \mathrm{Hz}^{1/2}/\mathrm{W}$ for a VO_2 bolometer, $3.2 \times 10^8\ \mathrm{cm} \cdot \mathrm{Hz}^{1/2}/\mathrm{W}$ for a Si bolometer at room temperature [17], $2.2 \times 10^{10}\ \mathrm{cm} \cdot \mathrm{Hz}^{1/2}/\mathrm{W}$ for a $GdBa_2Cu_3O_{7-x}$ bolometer at temperature of 85 K [18], and $6 \times 10^9\ \mathrm{cm} \cdot \mathrm{Hz}^{1/2}/\mathrm{W}$ for a Yba_2Cu3O_{7-x} bolometer at temperature of 90 K [19].

V. Conclusion

A new conceptual bolometer structure has been proposed and fabricated. Mechanically, the released membrane was suspended safely with a high flatness, and the signal bridge was driven well at a voltage of less than 10 V. Thermally, a thermal conductance as low as 4.13×10^{-8} W/K was achieved. As a result, the detectivity was estimated to be $4.23 \times 10^9\ \mathrm{cm} \cdot \mathrm{Hz}^{1/2}/\mathrm{W}$. The experimental results suggest a possibility of using the novel bolometer structure as an alternative to conventional bolometers. However, researches to solve some problems such as the good connection, the contact fatigue, and the negative TCR of the Ti film are still required to improve the reliability and the yield of the bolometer.

References

[1] M. Mansi, M. Brookfield, S. Porter, and I. Edwards, "A very low cost infrared detector and camera system," *Proc. SPIE*, vol. 4820, no. v.1, pp. 227–238, Jul. 2002.

[2] P. W. Kruse and D. D. Skatrud, *Uncooled Infrared Imaging Arrays and Systems*. San Diego, CA: Academic, 1997.

[3] A. Tanaka, S. Matsumoto, N. Tsukamoto, S. Itoh, K. Chiba, T. Endoh, A. Nakazato, K. Okuyama, Y. Kumazawa, M. Hijikawa, H. Gotoh, T. Tanaka, and N. Teranishi, "Influence of bias heating on titanium bolometer infrared sensor," *Proc. SPIE*, vol. 3061, no. pt.1, pp. 198–209, Apr. 1997.

[4] O. Degani, E. Socher, A. Lipson, T. Leitner, D. J. Setter, S. Kaldor, and Y. Nemirovsky, "Pull-in study of an electrostatic torsion microactuator," *J. Microelectromech. Syst.*, vol. 7, no. 4, pp. 373–379, Dec. 1998.

[5] H. Tilmans and R. Legtenberg, "Electrostatically driven vacuum encapsulated polysilicon resonators—Part II," *Sens. Actuators A, Phys.*, vol. 45, no. 1, pp. 67–84, Oct. 1994.

[6] R. Legtenberg, J. Gilbert, S. Senturia, and M. Elwenspoek, "Electrostatic curved electrode actuators," *J. Microelectromech. Syst.*, vol. 6, no. 3, pp. 257–265, Sep. 1997.

[7] M. W. Judy, Y. Cho, R. T. Howe, and A. P. Pisano, "Self-adjusting microstructures (SAMS)," in *Proc. MEMS*, 1991, pp. 51–56.

[8] T. Yasuda, I. Shimoyama, and H. Miura, "CMOS drivable electrostatic microactuator with large deflection," in *Proc. 10th MEMS Int. Workshop*, 1997, pp. 90–95.

[9] B. C. S. Chou, J. Shie, and C. Chen, "Fabrication of low-stress dielectric thin-film for microsensor applications," *IEEE Electron Device Lett.*, vol. 18, no. 12, pp. 599–601, Dec. 1997.

[10] F. Volklein, "Thermal conductivity and diffusivity of a thin film $SiO_2-Si_3N_4$ sandwich system," *Thin Solid Films*, vol. 188, no. 1, p. 27, Jul. 1990.

[11] O. Tabata, K. Kawahato, S. Sugiyama, and I. Igarashi, "Mechanical property measurements of thin films using load-deflection of composite rectangular membrane," *Sens. Actuators*, vol. 20, no. 1/2, pp. 135–141, Dec. 1989.

[12] S. T. Cho, K. Najafi, and K. D. Wise, "Scaling and dielectric stress compensation of ultrasensitive boron-doped silicon microstructures," in *Proc. IEEE Workshop Microelectromech. Syst.*, 1990, pp. 50–55.

[13] X. Gu, G. Karunasiri, J. Yu, G. Chen, U. Sridhar, and W. J. Zeng, "On-chip compensation of self-heating effects in microbolometer infrared detector arrays," *Sens. Actuators A, Phys.*, vol. 69, no. 1, pp. 92–96, Jun. 1998.

[14] A. Tanaka, S. Matsumoto, N. Tsukamoto, S. Itoh, K. Chiba, T. Endoh, A. Nakazato, K. Okuyama, Y. Kumazawa, M. Hijikawa, H. Gotoh, T. Tanaka, and N. Teranishi, "Influence of bias heating on titanium bolometer infrared sensor," *Proc. SPIE*, vol. 3061, no. v.1, pp. 198–209, Apr. 1997.

[15] J. Lijun and C. N. William, "Design, fabrication and testing of a micromachined thermo-optical light modulator based on a vanadium dioxide array," *J. Micromech. Microeng.*, vol. 14, no. 7, pp. 833–840, May 2004.

[16] P. C. Shan, Z. Celik-Butler, D. P. Butler, and A. Jahanzeb, "Semiconducting YBaCuO thin films for uncooled infrared bolometers," *J. Appl. Phys.*, vol. 78, no. 12, pp. 7334–7339, Sep. 1995.

[17] V. Y. Zerov and V. G. Malyarov, "Heat-sensitive materials for uncooled microbolometer arrays," *J. Opt. Technol.*, vol. 68, no. 12, pp. 939–948, Dec. 2001.

[18] S. Sanchez, M. Elwenspoek, C. Gui, M. de Nivelle, R. de Vries, P. de Korte, M. P. Bruijn, J. J. Wijnbergen, W. Michalke, E. Steinbeib, T. Heidenblut, and B. Schwierzi, "A high-Tc superconductor bolometer on a silicon nitride membrane," *J .Microelectromech. Syst.*, vol. 7, no. 1, pp. 62–68, Mar. 1998.

[19] J. C. Brasunas and B. Lakew, "High Tc superconductor bolometer with record performance," *Appl. Phys. Lett.*, vol. 64, no. 6, pp. 777–778, Feb. 1994.

Tae-Sik Kim received the M.S. and Ph.D. degrees in electrical engineering and computer science from the Korea Advanced Institute of Science and Technology (KAIST), Daejeon, Korea, in 1999 and 2006, respectively. His dissertation focused on developing a novel uncooled infrared detector.

From 1999 to 2002, he was with the Devices and Material Laboratory, LG Electronics Institute of Technology, working on optical MEMS. He is currently a Senior Member of the National NanoFab Center, KAIST, where he works in the area of biosensor and MEMS.

Hee Chul Lee received the B.S. degree in electronic engineering from the Seoul National University, Seoul, Korea, in 1978 and the M.S. and Ph.D. degrees from the Tokyo Institute of Technology, Tokyo, Japan, in 1986 and 1989, respectively.

Since 1989, he has been with the Department of Electrical Engineering and Computer Science, Korea Advanced Institute of Science and Technology, Daejeon, Korea, where he is currently a Professor. He has authored or coauthored more than 100 published papers in journals and conference proceedings. His research fields include high dielectric DRAM, infrared detector, and readout circuit.

Dr. Lee is a Program Committee Member of SPIE and an Adviser of Nikkei Nanotechnology. He was an Associate Editor of the *Japanese Journal of Applied Physics*. He has served as a Director of many conferences.